Inorganic Chemistry

ARTICLE

pubs.acs.org/IC

Luminescence Properties and Quenching Mechanisms of $Ln(Tf_2N)_3$ Complexes in the Ionic Liquid bmpyr Tf_2N

Amber Brandner, Taizo Kitahara, Nick Beare, Cuikun Lin, Mary T. Berry, and P. Stanley May*

Department of Chemistry, University of South Dakota, 414 East Clark Street, Vermillion, South Dakota 57069, United States

S *Supporting Information*

ABSTRACT: The emission properties, including luminescence lifetimes, of the lanthanide complexes $Ln(Tf_2N)_3$ (Tf_2N = bis(trifluoromethanesulfonyl)amide); Ln^{3+} = Eu^{3+}, Tm^{3+}, Dy^{3+}, Sm^{3+}, Pr^{3+}, Nd^{3+}, Er^{3+}) in the ionic liquid bmpyr Tf_2N (bmpyr = 1-*n*-butyl-1-methylpyrrolidinium) are presented. The luminescence quantum efficiencies, η, and radiative lifetimes, τ_R, are determined for $Eu^{3+}(^5D_0)$, $Tm^{3+}(^1D_2)$, $Dy^{3+}(^4F_{9/2})$, $Sm^{3+}(^4G_{5/2})$, and $Pr^{3+}(^3P_0)$ emission. The luminescence lifetimes in these systems are remarkably long compared to values typically reported for Ln^{3+} complexes in solution, reflecting weak vibrational quenching. The 1.5 μm emission corresponding to the Er^{3+} ($^4I_{13/2}\rightarrow{}^4I_{15/2}$) transition, for example, exhibits a lifetime of 77 μs. The multiphonon relaxation rate constants are determined for 10 different Ln^{3+} emitting states, and the trend in multiphonon relaxation is analyzed in terms of the energy gap law. The energy gap law does describe the general trend in multiphonon relaxation, but deviations from the trend are much larger than those normally observed for crystal systems. The parameters determined from the energy gap law analysis are consistent with those reported for crystalline hosts. Because Ln^{3+} emission is known to be particularly sensitive to quenching by water in bmpyr Tf_2N, the binding properties of water to Eu^{3+} in solutions of $Eu(Tf_2N)_3$ in bmpyr Tf_2N have been quantified. It is observed that water introduced into these systems binds quantitatively to Ln^{3+}. It is demonstrated that $Eu(Tf_2N)_3$ can be used as a reasonable internal standard, both for monitoring the dryness of the solutions and for estimating the quantum efficiencies and radiative lifetimes for visible-emitting $[Ln(Tf_2N)_x]^{3-x}$ complexes in bmpyr Tf_2N.

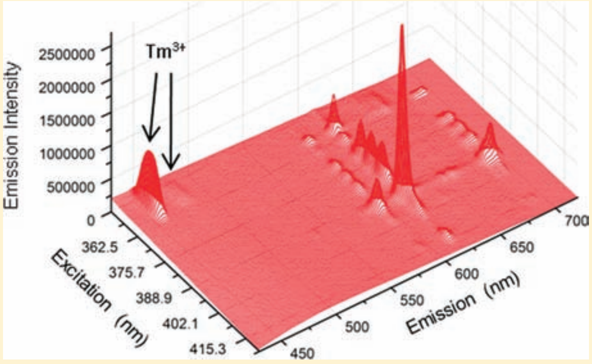

1. INTRODUCTION

Lanthanide ions have long been arguably the most important class of luminescent materials in society, being the key activators in fluorescent lighting, lasers, and optical telecommunications systems.[1−3] Moreover, in spite of advances made in alternative phosphors, such as organic and inorganic semiconductors, technological and scientific interest in lanthanide-based luminescent materials continues to grow. A recent review gives an excellent overview of the current research trends in this area, which include sensitization of near-infrared (NIR) emission; development of "soft materials", such as liquid crystals, ionic liquids (ILs), and ionogels; electroluminescent materials for use in organic light-emitting devices (OLEDS); and applications in biosensing and bioimaging.[4] The use of ILs as optical materials is an example of an increasing focus on ILs in materials research.[5]

Recent studies on the luminescence properties of lanthanide complexes in ILs have shown that ILs have unique advantages as matrixes for luminescent lanthanide ions.[6−22] Using ILs with weakly coordinating anions, it is possible to study the optical properties of lanthanides complexes with weakly binding ligands. Also, multiphonon relaxation (i.e., vibrational quenching) in many IL systems appears to be less efficient relative to that observed in conventional solvents. For example, strong NIR emission has been reported for lanthanide complexes in several IL matrixes.[13,16,17] Also, Babai, et al. have reported strong emission from the $^3P_0$ state of Pr^{3+} in solutions of $Pr(Tf_2N)_3$ (Tf_2N = bis(trifluoromethanesulfonyl)amide) in bmpyr Tf_2N (bmpyr = 1-*n*-butyl-1-methylpyrrolidinium), noting that it is very rare to observe $Pr^{3+}(^3P_0)$ emission from solution.[15] It is this report that prompted us to undertake a systematic study of the luminescence properties of $Ln(Tf_2N)_3$ in bmpyr Tf_2N. It was clear to us that, if $Pr^{3+}(^3P_0)$ emission could be observed in this system, then it should be possible to observe emission from many different Ln^{3+} excited states, offering the rare opportunity to perform a systematic study of the multiphonon relaxation behavior across a series of emitting levels in a fluid system. Such studies are normally possible only for lanthanides in crystalline or glass hosts.

Here, we present the emission properties, including luminescence lifetimes, of $Ln(Tf_2N)_3$ (Ln^{3+} = Eu^{3+}, Tm^{3+}, Dy^{3+}, Sm^{3+}, Pr^{3+}, Nd^{3+}, Er^{3+}) in bmpyr Tf_2N. The luminescence quantum efficiencies, η, and radiative lifetimes, τ_R, are determined for $Eu^{3+}(^5D_0)$, $Tm^{3+}(^1D_2)$, $Dy^{3+}(^4F_{9/2})$, $Sm^{3+}(^4G_{5/2})$, and $Pr^{3+}(^3P_0)$ emission. The

Received: December 20, 2010
Published: June 15, 2011

multiphonon relaxation rate constants are determined for 10 different Ln^{3+} emitting states, and the trend in multiphonon relaxation is analyzed in terms of the energy gap law. Also, because Ln^{3+} emission is known to be particularly sensitive to quenching by water in weakly coordinating ILs, such as bmpyr Tf_2N, we have quantitatively analyzed the binding properties of water to Eu^{3+} in solutions of $Eu(Tf_2N)_3$ in bmpyr Tf_2N. It is demonstrated that $Eu(Tf_2N)_3$ can be used as a reasonable internal standard both for monitoring the dryness of the solutions, and for estimating the quantum efficiencies and radiative lifetimes for visible-emitting $[Ln(Tf_2N)_x]^{3-x}$ complexes in bmpyr Tf_2N.

It is observed that the Ln^{3+} luminescence lifetimes in these systems are, in general, remarkably long compared to values typically reported for Ln^{3+} complexes in solution, reflecting weak vibrational quenching. The 1.5 μm emission corresponding to the Er^{3+} ($^4I_{13/2}{\to}^4I_{15/2}$) transition, for example, exhibits a lifetime of 77 μs. The overall trend in multiphonon relaxation across the series of emitting states does generally follow the energy gap law, but a much greater degree of fluctuation from the best-fit trend is seen than is typically observed for Ln^{3+} in solid-state hosts. The parameters obtained from an energy-gap-law analysis are consistent with those reported for well-known crystal systems. The strength of coupling to the active vibrational mode in the $[Ln(Tf_2N)_x]^{3-x}$ complex is very similar to that observed for Ln^{3+} in Y_2O_3. In addition, a comparison of the present results with those in the literature for other IL systems suggests that vibrational quenching of Ln^{3+} emission by the IL cation could be the dominant quenching mechanism when the first coordination sphere of the Ln^{3+} complex is small.

2. EXPERIMENTAL SECTION

2.1. Chemicals. All lanthanide oxides were from the American Potash & Chemical Company (99.9%), except for europium oxide, which was purchased from Alfa Aesar (99.9%). HTf_2N (>95%) was purchased as a powder from Fluka. Rhodamine 590 chloride (R6G) was purchased from Exciton. Quinine sulfate (QS) was purchased from Mallinckrodt. Solutions of $Ln(Tf_2N)_3$ in bmpyr Tf_2N were made from a single lot of bmpyr Tf_2N purchased from Fluka (Product-No 38894/Lot 1346087), except for the mixed solutions of Sm/Eu, Pr/Eu, and Dy/Eu, which were made using bmpyr Tf_2N purchased from EMD (Product No. 4-91046/Lot L57164146). The IL from Fluka had a water content <50 ppm (Karl Fischer) and a total halide content of <25 ppm (ion chromatography). The IL from EMD had a water content <100 ppm - (Karl Fischer) and a total halide content of <100 ppm (ion chromatography). The bmpyr Tf_2N used in this study was clear in appearance and exhibited a faint blue emission when excited with UV light.

2.2. Synthesis of $Ln(Tf_2N)_3$. Powders of $Ln(Tf_2N)_3$ were synthesized by reacting the Ln_2O_3 with a slight excess of HTf_2N. Typically, Ln_2O_3 (0.06 g) and HTf_2N (0.31 g) were combined in a Vycor ampule and ~3 mL of nanopure water was added dropwise to the mixture. The resulting $Ln(Tf_2N)_3$ was heated over sand slowly, bringing the mixture to a gentle boil, resulting in a clear homogeneous mixture. The sample was then heated at 100 °C under vacuum (20−50 mTorr) for 5−12 h until a dry powder was obtained. The composition of the product was confirmed by elemental analysis.

2.3. Preparation of Solutions of $Ln(Tf_2N)_3$ in bmpyr Tf_2N. A Vycor ampule was prepared by heating with a hydrogen−oxygen torch under vacuum to remove any moisture present inside the ampule. The evacuated Vycor ampule, along with the $Ln(Tf_2N)_3$ sample, was transferred into a controlled-atmosphere glovebox. The IL, bmpyr Tf_2N, and $Ln(Tf_2N)_3$ were combined in the ampule. The resulting $Ln(Tf_2N)_3$ in bmpyr Tf_2N was clear and appeared to be slightly more viscous than the pure IL. The Vycor ampule was then connected to a hose with a two-way valve to protect the solution from atmosphere upon removal from the glovebox. The solution was then dried under vacuum (20−50 mTorr) at 150−180 °C for 12−24 h. A liquid nitrogen trap was used between the sample and the two-stage, rotary-vane pump to protect the sample from contamination. The ampule was then sealed using a hydrogen−oxygen torch while still under vacuum. All solution concentrations are reported in units of mol % $Ln(Tf_2N)_3$ in bmpyr Tf_2N.

2.4. Spectroscopic Measurements. All spectroscopic data presented here were acquired at room temperature unless otherwise indicated. For 77 K measurements, samples previously sealed under vacuum in Vycor ampules were slowly lowered into an optical quartz dewar, which was half-filled with liquid nitrogen, until the tip of the ampule was in contact with the cryogen. For 77 K measurements, the samples were in a glass-like state. If significant cracking, or other signs of crystallization were observed, the measurements were discontinued.

Visible emission and excitation spectra were acquired on a Fluoromax or Flouromax-4 fluorometer (JY Horiba). All spectra are corrected for instrument response in terms of relative photon flux per wavelength interval. Emission spectra for quantum efficiency measurements were also corrected for the intensity of the excitation light. Near infrared emission spectra and lifetime measurements were acquired using a NIR-PMT (Hamamatsu, H10330−75) mounted on the lateral port of a 1/3 m flat-field monochromator (JY Horiba, TRIAX 320). The signal from the NIR-PMT was amplified using a single channel (5×) of a preamplifier (Stanford Research Systems, SR 445A) and then fed to a multichannel scalar (Stanford Research Systems, SR 430) for time-resolved photon counting. The detection system was calibrated for relative wavelength response using a standard Tungsten lamp with extended calibration out to 1700 nm. (Stellar Net, SL1-CAL).

Luminescence lifetimes visible emission were acquired using a 0.46 M flat-field monochromator (Jobin-Yvon HR460), and a time-resolved photon-counting detection system consisting of a fast, red-sensitive, side-window photomultiplier (Hamamatsu R2949). To obtain the lifetime of Pr^{3+} ($^3P_0$) emission, a digital oscilloscope (Tektronix, TDS 2022) was used in place of the multichannel scalar for improved time resolution.

The pulsed excitation source for lifetime measurements was provided by either a nitrogen laser/dye laser system (Laser Photonics, models UV-12 and DL-14, respectively) or an optical parametric oscillator (Opotek, Opolette).

2.5. Water Binding Measurements. Three trials were performed adding controlled increments of water to $Eu(Tf_2N)_3$ in bmpyr Tf_2N. 1.0 μL increments of nanopure water were added to 2.93 g of 1.07% $Eu(Tf_2N)_3$ in bmpyr Tf_2N, 3.10 g of 1.04% $Eu(Tf_2N)_3$ in bmpyr Tf_2N and 1.58 g of 1.28% $Eu(Tf_2N)_3$ in bmpyr Tf_2N, respectively. One additional trial was performed by adding 1 μL increments of D_2O to 3.08 g of 1.08% $Eu(Tf_2N)_3$ in bmpyr Tf_2N. Prior to the addition of water, each sample was transferred from its ampule to a cuvette with a septum top inside a glovebox. The increments of water/D_2O were added to $Eu(Tf_2N)_3$ in bmpyr Tf_2N through the septum top of the cuvette using a 10 μL Hamilton syringe. After each addition of water/D_2O, the sample was left to stir on a magnetic stirrer for 5 min prior to optical measurements.

3. RESULTS AND DISCUSSION

3.1. Quantum Efficiency and Radiative Lifetime Measurements for $Ln(Tf_2N)_3$ in bmpyr Tf_2N. The luminescence quantum efficiency, η, of an emitting species in solution can be estimated by comparison to a secondary standard with a known quantum efficiency according to[23,24]

$$\eta = \eta_{\mathrm{std}} \frac{I}{I_{\mathrm{std}}} \cdot \left(\frac{n}{n_{\mathrm{std}}}\right)^2 \cdot \frac{A_{\mathrm{std}}}{A} \qquad (1)$$

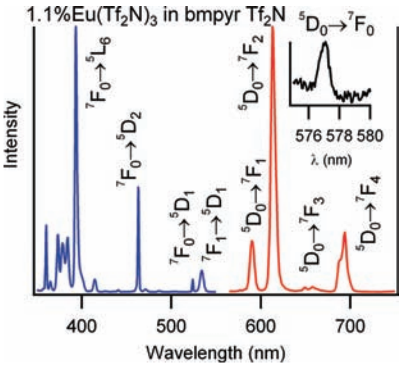

Figure 1. Emission (red) and excitation (blue) spectra of Eu^{3+} in 1.1% $Eu(Tf_2N)_3$ in bmpyr Tf_2N. (λ_{ex} = 394 nm, λ_{em} = 614 nm) Spectral resolution is 1 nm. Spectra are corrected for instrument response.

where η and η_{std} are the quantum efficiencies of the sample and the secondary standard, respectively; I and I_{std} are the integrated intensities of the corrected emission spectra of the sample and secondary standard, respectively; n and n_{std} are the refractive indices of the solvent for the sample and standard solutions, respectively; and A_{std} and A are the absorbance of the standard and sample, respectively, at the excitation wavelengths used to acquire the emission spectra. Equation 1 is appropriate for optically dilute solutions for which the absorbance at the excitation and emission wavelengths is ≤0.05. There are really no ideal common secondary standards for the determination of the quantum efficiencies of luminescent Ln^{3+} ions,[25,26] partly because Ln^{3+} ions exhibit sharp-line spectra, whereas the well-established secondary standards are organic dyes with very broad spectral bands. Although the use of Ln^{3+}-based secondary standards has been suggested,[26] the practice has not yet gained wide acceptance.

In the present study, we use Rhodamine 590 (R6G) in ethanol (η = 0.94)[27] and quinine sulfate (QS) in 1 N H_2SO_4 (η = 0.546)[23,28] as common secondary standards to determine the quantum efficiencies of $Ln(Tf_2N)_3$ in bmpyr Tf_2N. In addition, however, we also calculate the quantum efficiencies of $Ln(Tf_2N)_3$ in bmpyr Tf_2N using $Eu(Tf_2N)_3$ as an internal secondary standard in the IL solution. As discussed below, the η_{std} for $Eu(Tf_2N)_3$ can be determined from a corrected emission spectrum and the measured lifetime of $Eu(Tf_2N)_3$.

In some instances, the absorbance of the IL solutions exceeded 0.05, either because of the intrinsic absorbance of the Ln^{3+} complex or because of baseline absorbance of the IL itself. In such cases, the integrated luminescence intensity of the sample was corrected for inner filter effects using the method of Parker and Barnes,[29] which has been shown to be very effective.[30]

Although the quantum efficiencies of $Ln(Tf_2N)_3$ in bmpyr Tf_2N are of intrinsic interest, they also permit us to calculate the associated radiative lifetimes, τ_R, of the luminescent species according to

$$\tau_R = \frac{\tau}{\eta} \qquad (2)$$

where τ is the measured luminescence lifetime. The value of τ_R and τ can then be used to calculate the nonradiative contribution to τ. As will be discussed below, the values of τ_R obtained using $Eu(Tf_2N)_3$ as an internal secondary standard are consistent with those obtained using R6G or QS.

3.2. Luminescence Properties, Quantum Efficiency, and Radiative Lifetime of Eu^{3+} in $Eu(Tf_2N)_3$ in bmpyr Tf_2N.

The emission and excitation spectra of 1% $Eu(Tf_2N)_3$ in bmpyr Tf_2N are shown in Figure 1. Peaks in the emission and excitation spectra are indicated according to the $^{2S+1}L_J$ Russell–Saunders labels for the initial and final multiplet states of the optical transitions. The peak corresponding to the $^5D_0 \rightarrow {}^7F_0$ emission, which is too weak to see clearly in the survey emission spectrum, is expanded and shown in the upper right inset of Figure 1.

The asymmetry factor, R, which is the ratio of the integrated intensity of the $^5D_0 \rightarrow {}^7F_2$ transition to the $^5D_0 \rightarrow {}^7F_1$ transition, is 5.4. R is useful for making qualitative comparisons of the Eu^{3+} chemical environment, because R tends to increase as the site symmetry lowers and as ligand polarizability increases.[31] The observation of only one electronic origin in the $^5D_0 \rightarrow {}^7F_0$ region indicates that there is probably only one Eu^{3+} species present in the anhydrous solution. Model Ln^{3+} compounds, which give some insight as to possible structures for Ln^{3+} complexes in IL solutions, have been synthesized from the reaction of lanthanide salts with ILs.[15,32−36] Babai, et al. were able to crystallize the compound $[bmpyr]_2[Pr(Tf_2N)_5]$ from a concentrated solution of $Pr(Tf_2N)_3$ in bmpyr Tf_2N and showed that the $[Pr(Tf_2N)_5]^{2-}$ complex is a distorted monocapped square antiprism in which the Pr^{3+} ion has a coordination number of 9.[15] For $[bmpyr]_2[Eu(Tf_2N)_5]$, Tang, et al. describe the coordination environment of Eu^{3+} (in the solid state) as a distorted tricapped trigonal prism (which is also a monocapped square antiprism) in which Eu^{3+} has a coordination number of 9.[8] The synthesis and crystal structures of $[bmpyr]_2[Ln(Tf_2N)_5]$, Ln = Nd, Tb, and $[bmpyr][Ln(Tf_2N)_4]$, Ln = Tm, Lu, have also been reported.[33] In addition, the compound $[bmim][Y(Tf_2N)_4]$ (bmim = 1-butyl-3-methylimidazolium) was obtained from the IL $[bmim][Tf_2N]$ and $Y(Tf_2N)_3$.[32] The oxygen coordination polyhedron around Y^{3+} is described as a trigonal dodecahedron. There is some evidence, however, that, in the liquid state of Tf_2N-based ILs, the coordination number of Eu^{3+} could be as high as 10.[8,14]

The corrected emission spectrum in Figure 1 was used to estimate the radiative lifetime of $Eu^{3+}(^5D_0)$. This method is based on using the known radiative rate constant for the $^5D_0 \rightarrow {}^7F_1$ magnetic-dipole transition, which is largely unaffected by the crystal-field, as an internal reference in a corrected emission spectrum to determine the total radiative lifetime.[37−39] The radiative lifetime, τ_R, is given by[39]

$$\frac{1}{\tau_R} = A_{MD,0} n^3 \left(\frac{I_{tot}}{I_{MD}} \right) \qquad (3)$$

where $A_{MD,0}$ is the Einstein spontaneous emission coefficient for the $^5D_0 \rightarrow {}^7F_1$ magnetic-dipole transition (in vacuum), n is the refractive index of the medium, and I_{tot} and I_{MD} are the integrated intensities of the total emission spectrum and the $^5D_0 \rightarrow {}^7F_1$ magnetic-dipole transition peak, respectively. The value for $A_{MD,0}$ is taken as 14.65 s^{-1},[39] and the refractive index of bmpyr Tf_2N is reported at 1.423.[40] From the emission spectrum in Figure 1, it was determined that (I_{tot}/I_{MD}) = 8.18. Applying eq 3, the radiative lifetime of $Eu^{3+}(^5D_0)$ was estimated to be τ_R = 2.90 ± 0.41 ms. The uncertainty given for τ_R is the most probable error calculated assuming a 10% uncertainty in the experimental determination of both I_{tot} and I_{MD}.

As an independent check on the value of τ_R, we measured the quantum efficiency of a solution of 4% $Eu(Tf_2N)_3$ in bmpyr

Table 1. Calculated Values of the Quantum Efficiency, η_{Ln}, and Radiative Lifetime, τ_R^{Ln}, of Ln^{3+} = Eu^{3+}, Tm^{3+}, Sm^{3+}, Pr^{3+}, Dy^{3+} Emission of $Ln(Tf_2N)_3$ in bmpyr Tf_2N Using eqs 1 and 2[a]

Ln^{3+}	standard	I_{Ln}/I_{std}	$A_{Ln}(\lambda)$	$A_{std}(\lambda)$	τ_{Ln}	η_{Ln}	τ_R^{Ln}
$Eu^{3+}(^5D_0)$	R6G in EtOH	0.539	0.046 (463 nm)	0.036 (480 nm)	1.22 ms	0.442 ± 0.088	2.75 ± 0.55 ms
$Tm^{3+}(^1D_2)$	QS in 1N H_2SO_4	0.251	0.028 (358 nm)	0.037 (358 nm)	6.32 μs	0.209 ± 0.042	30.2 ± 6.0 μs
$Sm^{3+}(^4G_{5/2})$	R6G in EtOH	0.0360	0.022 (480 nm)	0.036 (480 nm)	300. μs	0.060 ± 0.012	5.0 ± 1.0 ms
$Pr^{3+}(^3P_0)$	R6G in EtOH	0.00247	0.071 (480 nm)	0.036 (480 nm)	78.7 ns	0.00131 ± 0.00026	59 ± 12 μs
$Dy^{3+}(^4F_{9/2})$	R6G in EtOH	0.0677	0.021 (453 nm)	0.036 (480 nm)	140. μs	0.122 ± 0.024	1.14 ± 0.23 ms

[a] Either Rhodamine 6G (R6G) in ethanol (η = 0.94) or quinine sulfate (QS) in 1 N H_2SO_4(aq) (η = 0.546) were used as a secondary standard, as indicated. The relevant input values for eqs 1 and 2 are also included. A_{Ln} and A_{std} were measured at the excitation wavelengths listed in brackets. The uncertainties reported for η_{Ln} and τ_R^{Ln} are the most probable errors calculated using assuming a 10% uncertainty in the determination of each I and A value. The uncertainties in the fitted values of τ_{Ln} were outside the significant figures reported here, and made no contributions to the propagated errors.

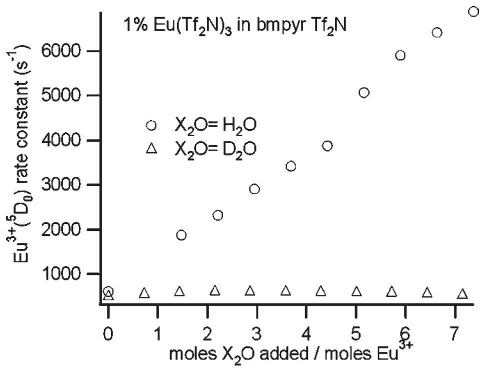

Figure 2. Plot of rate constants for $Eu^{3+}(^5D_0)$ relaxation for 1% $Eu(Tf_2N)_3$ in bmpyr Tf_2N as a function of added X_2O (X = H, D) relative to the moles of Eu^{3+} present in the sample.

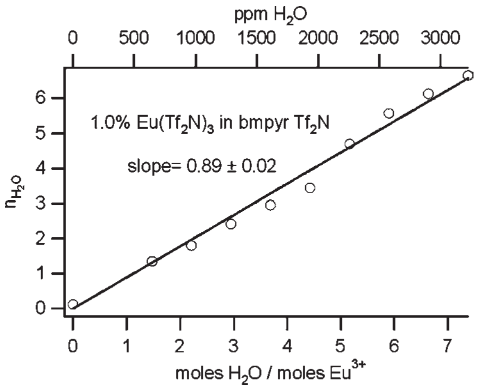

Figure 3. Plot of average number of moles of water bound to Eu^{3+}, n_{H2O}, as a function of the ratio of moles of added water to moles of Eu^{3+} present in a solution of 1% $Eu(Tf_2N)_3$ in bmpyr Tf_2N. The value of n_{H2O} was determined using eq 4, and the data shown in Figure 2. The absolute concentration of added water in solution is shown on the top horizontal axis.

Tf_2N against a secondary standard of R6G in ethanol (See Table 1). The quantum efficiency of $Eu^{3+}(^5D_0)$ emission in 4% $Eu(Tf_2N)_3$ in bmpyr Tf_2N was determined to be $\eta = 0.442 \pm 0.088$. The measured lifetime of the $Eu^{3+}(^5D_0)$ emission in this same solution was τ = 1.22 ms, which corresponds to $\tau_R = 2.75 \pm 0.55$ ms (Table 1). This value is within the estimated error of $\tau_R = 2.90 \pm 0.41$ ms, determined using the corrected emission spectrum and eq 3.

The value of η for $Eu(Tf_2N)_3$ in bmpyr Tf_2N varies with water content at the parts per million level. The quantum efficiency in any given solution can now be estimated using the observed lifetime of $Eu^{3+}(^5D_0)$ emission and the relation $\eta = \tau/\tau_R$, where $\tau_R = 2.90 \pm 0.41$ ms. Based on the luminescence lifetimes of $Eu^{3+}(^5D_0)$ measured for multiple solutions of $Eu(Tf_2N)_3$ in bmpyr Tf_2N (discussed below), the quantum efficiency, η, of $Eu^{3+}(^5D_0)$ emission in these samples ranged from 0.38 to 0.69. The ability to determine the quantum efficiency and radiative lifetime of $Eu^{3+}(^5D_0)$ emission in our IL solutions allows us to use $Eu(Tf_2N)_3$ as an internal secondary standard for estimating the quantum efficiencies and radiative lifetimes for other $Ln(Tf_2N)_3$ complexes in bmpyr Tf_2N.

3.3. Binding Properties of Water to Ln^{3+} in Solutions of $Ln(Tf_2N)_3$ in bmpyr Tf_2N. The luminescence efficiency of lanthanide ions in Tf_2N-based ILs is very sensitive to the presence of water.[11,13,15,16,18] We were interested in quantifying the binding properties of water to Ln^{3+} in solutions of $Ln(Tf_2N)_3$ in bmpyr Tf_2N to more fully understand the quenching effects of water content on Ln^{3+} emission. Moreover, if the quenching properties can be quantitatively related to water content, it should be possible to use Ln^{3+} emission as a probe of water content.

The observed decay constant of $Eu^{3+}(^5D_0)$ emission can be used to estimate the average number of waters, n_{H2O}, in the first coordination sphere of Eu^{3+} according to the following equation[41]

$$n_{H_2O} = 1.05 \times 10^{-3}(k_{H_2O} - k_{D_2O}) \qquad (4)$$

where k_{H2O} and k_{D2O} are the observed decay constant (in s^{-1}) of $Eu^{3+}(^5D_0)$ emission in the presence of H_2O and D_2O, respectively. The difference in k_{H2O} and k_{D2O} is assumed to represent the rate constant for quenching by water. Equation 4 is generally considered to be accurate to ±0.5 waters. We note that we have not applied an updated version of eq 4,[42] because it includes contributions to quenching from 'bulk' water outside the primary coordination sphere, which is not appropriate to the present systems.

Figure 2 shows the fitted values of k_{H_2O} and k_{H_2O} as a function of X_2O (X = H or D) added to a solution of 1% $Eu(Tf_2N)_3$ in bmpyr Tf_2N. The amount of X_2O added is expressed in terms of moles of X_2O per mole of Eu^{3+} present in solution. Note that k_{H_2O} increases linearly with added H_2O.

The data in Figure 2 can be transformed, using eq 4, to show the average number of waters bound to Eu^{3+} as a function of the ratio of moles of added water per mole of Eu^{3+} in solution (See Figure 3). The absolute concentration of added water (ppm) is shown on the upper horizontal axis of Figure 3. Figure 3 shows that a linear fit of n_{H_2O} versus moles added H_2O per mole of

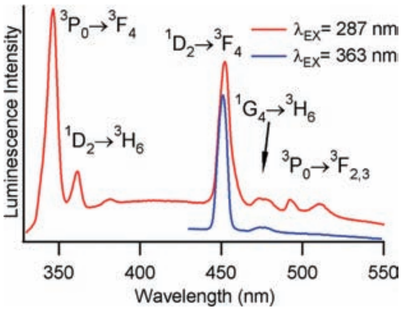

Figure 4. Emission spectrum of Tm^{3+} in 0.5%$Tm(Tf_2N)_3$/0.6%$Eu(Tf_2N)_3$ in bmpyr Tf_2N exciting at 287 nm (red) and at 363 nm (blue). Spectral resolution is 2 nm. Spectra are corrected for instrument response.

Eu^{3+} yields a slope of 0.89 ± 0.02. Repeating this experiment three times for three different samples yielded an average slope of 1.0 ± 0.2. The interpretation of these results is clear; *the added water is binding quantitatively to* Eu^{3+}. This implies that there is no water-content threshold in these IL solutions below which direct coordination to Ln^{3+} (and, therefore, quenching) does not occur. This is in stark contrast to the case of solutions of $LnCl_3$ in the IL 1-butyl-3-methylimidazolium chloride (bmimCl) in which it has been shown that no direct binding of water to Ln^{3+} occurs until a 1:1 ratio of moles of water to moles of bmimCl is reached.[10] In bmpyr Tf_2N, the weakly coordinating Tf_2N^- anions cannot compete with even a trace presence of water.

We note that the solutions tended to become somewhat inhomogeneous at ratios of moles of water to moles of Eu^{3+} higher than 6 because of the formation of an emulsion. O'Mahony et al. report that the water saturation level of bypyr Tf_2N at 298 K is 11,407 ppm,[43] which is far above the water content levels used in this study. We suggest, therefore, that the phase segregation has been hastened by the presence of Eu^{3+} in the IL. Billard et al. report the formation of a water emulsion in nondegassed solutions of europium triflate in bmim Tf_2N.[18] The lifetimes reported for these samples clearly indicate that Eu^{3+} has segregated into the aqueous phase of the emulsion.

Our results indicate that $Eu(Tf_2N)_3$ can be used as a spectroscopic probe of water content in bmpyr Tf_2N. Decay curves of $Eu^{3+}(^5D_0)$ emission can be used to determine the molar ratio of water to Eu^{3+}, which, in turn, can be used to determine the absolute water content of the IL, if the $Eu(Tf_2N)_3$ concentration is accurately known.

In fact, we can use this method to establish an upper limit on the water content of our as-prepared solutions of $Eu(Tf_2N)_3$ in bmpyr Tf_2N. Prior to the addition of water, the $Eu^{3+}(^5D_0)$ lifetime of the $Eu(Tf_2N)_3$ solution represented in Figures 2 and 3 was 1.62 ms ($k = 616$ s^{-1}). Using the value of the radiative decay constant $k_R = 345$ s^{-1} (See section 3.2), the total nonradiative rate constant, k_{NR}, is $k_{NR} = 271$ s^{-1}. If k_{NR} is entirely attributable to quenching by water, then $k_{NR} = k_{H2O} - k_{D2O}$ and $n_{H2O} = mole_{H2O}/mole_{Eu^{3+}} = 0.28$ (See eq 4). Therefore, the *maximum* water concentration in the original solution of 1% $Eu(Tf_2N)_3$ in bmpyr Tf_2N is 0.28 mol % (or 120 ppm).

3.4. Luminescence Properties, Quantum Efficiency, and Radiative Lifetime of $Tm^{3+}(^1D_2)$ in $Tm(Tf_2N)_3$ in bmpyr Tf_2N.

The luminescence spectra of Tm^{3+} in 0.5% $Tm(Tf_2N)_3$/0.6% $Eu(Tf_2N)_3$ in bmpyr Tf_2N are shown in Figure 4. Identical spectra were obtained from solutions containing no $Eu(Tf_2N)_3$.

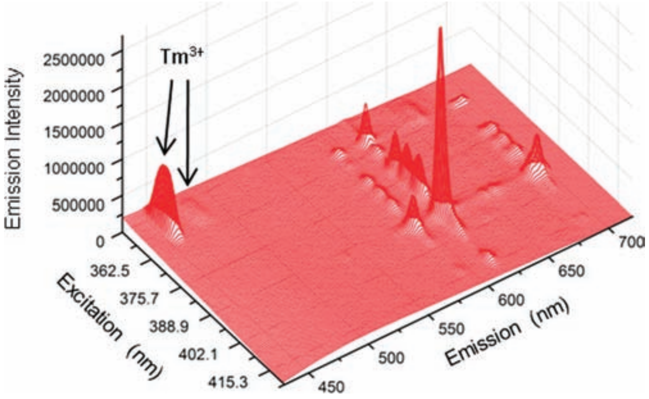

Figure 5. 3D Emission/Excitation mapping of the luminescence properties of 0.5% $Tm(Tf_2N)_3$ and 0.6% $Eu(Tf_2N)_3$ in bmpyr Tf_2N. Resolution of emission and excitation is 1 nm.

Co-doping the Tm^{3+} solution with Eu^{3+} enabled us both to ensure that the solution was dry (from the $Eu^{3+}(^5D_0)$ decay curves) and to estimate the quantum efficiency of $Tm^{3+}(^1D_2)$ emission using Eu^{3+} as an internal secondary standard.

The two spectra shown in Figure 4 were obtained using 287 nm excitation (red spectrum) and 363 nm excitation (blue spectrum). Transitions from three distinct emitting states of Tm^{3+} are clearly observed: $^3P_0$ (34,770 cm^{-1}), $^1D_2$ (27,840 cm^{-1}), and $^1G_4$ (21,200 cm^{-1}). The 363 nm excitation results in emission from the $^1D_2$ and $^1G_4$ states (blue spectrum), while 287 nm excitation results in emission from all three states.

A partial 3D emission-excitation matrix of the mixed solution is shown in Figure 5. The major Tm^{3+} emission peaks are marked. No evidence of energy transfer between Tm^{3+} and Eu^{3+} is observed. The maximum Tm^{3+} absorbance in the excitation range shown is 0.012 at 363 nm, while the maximum Eu^{3+} absorbance is 0.026 at 394 nm. It is clear by inspection, therefore, that the quantum efficiency of Tm^{3+} emission is reasonably high, because the Tm^{3+} emission is not dwarfed by the Eu^{3+} emission.

The quantum efficiency, η, and radiative lifetime, τ_R, of $Tm^{3+}(^1D_2)$ emission were estimated using eqs 1 and 2, respectively, relative to two different secondary standards: quinine sulfate (QS) in 1 N H_2SO_4 and $Eu(Tf_2N)_3$ in bmpyr Tf_2N. For a solution of 1% $Tm(Tf_2N)_3$ in bmpyr Tf_2N against a QS standard, it was determined that $\eta = 0.209 \pm 0.042$ and $\tau_R = 30.2 \pm 6.0$ μs (See Table 1). For a solution of 0.5% $Tm(Tf_2N)_3$/0.6% $Eu(Tf_2N)_3$ in bmpyr Tf_2N against the internal $Eu(Tf_2N)_3$ standard, it was determined that $\eta = 0.229 \pm 0.046$ and $\tau_R = 27.5 \pm 5.5$ μs (See Table 2). For both determinations, the spectrum obtained using λ_{ex} = 287 nm (Figure 4) was used to estimate the contribution of the $Tm^{3+}(^1D_2 \rightarrow {}^3H_6)$ transition to the integrated intensity, I (See eq 1). The values of τ_R and η obtained using the two standards are in quite good agreement. We note that it is more meaningful, in general, to compare τ_R values from the two different methods, because τ (and, therefore, η) varies somewhat from solution to solution because of slight differences in dryness (See Table 3). In this particular case, both τ_R and η are in agreement, because the measured lifetime of $Tm^{3+}(^1D_2)$ is quite similar in both solutions.

In spite of the relatively short lifetime of $Tm^{3+}(^1D_2)$, the quantum efficiency of $Tm^{3+}(^1D_2)$ emission is quite high, being approximately one-half that observed for $Eu^{3+}(^5D_0)$ emission.

Table 2. Calculated Values of the Quantum Efficiency, η_{Ln}, and Radiative Lifetime, τ_R^{Ln}, of Ln^{3+}= Tm^{3+}, Sm^{3+}, Pr^{3+}, Dy^{3+} Emission in Solution of $\mathrm{Ln(Tf_2N)_3/Eu(Tf_2N)_3}$ in bmpyr $\mathrm{Tf_2N}$ Using eqs 1 and 2[a]

Ln^{3+}	$I_{\mathrm{Ln}}/I_{\mathrm{Eu}}$	$A_{\mathrm{Ln}}(\lambda)$	$A_{\mathrm{Eu}}(\lambda)$	τ_{Eu} (ms)	τ_R^{Eu}(ms)	τ_{Ln}	η_{Eu}	η_{Ln}	τ_R^{Ln}
$\mathrm{Tm}^{3+}(^1\mathrm{D}_2)$	0.246	0.012 (363 nm)	0.026 (394 nm)	1.24	2.90 ± 0.41	6.29 μs	0.430 ± 0.060	0.229 ± 0.046	27.5 ± 5.5 μs
$\mathrm{Sm}^{3+}(^4\mathrm{G}_{5/2})$	0.452	0.182 (402 nm)	0.070 (394 nm)	1.59	2.90 ± 0.41	430. μs	0.548 ± 0.078	0.095 ± 0.019	4.53 ± 0.91 ms
$\mathrm{Pr}^{3+}(^3\mathrm{P}_0)$	0.0163	0.406 (444 nm)	0.094 (394 nm)	1.11	2.90 ± 0.41	81.3 ns	0.384 ± 0.054	$(1.78 \pm 0.36)\mathrm{x}10^{-3}$	45.6 ± 9.1 μs
$\mathrm{Dy}^{3+}(^4\mathrm{F}_{9/2})$	0.219	0.010 (451 nm)	0.014 (464 nm)	1.10	2.90 ± 0.41	187 μs	0.381 ± 0.054	0.122 ± 0.024	1.53 ± 0.31 ms

[a] The relevant input values for eqs 1 and 2 are also included. A_{Ln} and A_{Eu} were measured at the excitation wavelengths which are listed in brackets. The uncertainties reported for η_{Ln} and $\tau_R^{Ln}$are the most probable errors calculated using the reported error in τ_R^{Eu} and assuming a 10% uncertainty in the determination of each I and A value. The uncertainties in the fitted values of τ_{Eu} and τ_{Ln} were outside the significant figures reported here, and made no contributions to the propagated errors.

This is due to the relatively short radiative lifetime of Tm^{3+}($^1\mathrm{D}_2$), τ_R^{Tm}. Jayasankar et al. have compiled an extensive table of radiative lifetimes for $\mathrm{Tm}^{3+}(^1\mathrm{D}_2)$ in crystal and glass matrixes, with τ_R^{Tm} ranging from 6 to 148 μs.[44] Our calculated value of τ_R^{Tm} is consistent with this range. As an interesting comparison, Weber reports a radiative lifetime of 17 μs and a quantum efficiency of 53% for $\mathrm{Tm}^{3+}(^1\mathrm{D}_2)$ emission in the $\mathrm{Y_2O_3}$(s) lattice.[45] The quantum efficiency of $\mathrm{Tm}^{3+}(^1\mathrm{D}_2)$ emission in bmpyr $\mathrm{Tf_2N}$, therefore, is comparable to that observed for solid-state systems.

3.5. Luminescence Properties, Quantum Efficiency, and Radiative Lifetime of $\mathrm{Sm}^{3+}(^4\mathrm{G}_{5/2})$ in $\mathrm{Sm(Tf_2N)_3}$ in bmpyr $\mathrm{Tf_2N}$.

A partial three-dimensional (3D) emission-excitation matrix for 2% $\mathrm{Sm(Tf_2N)_3}$/2%$\mathrm{Eu(Tf_2N)_3}$ in bmpyr $\mathrm{Tf_2N}$ is shown in Figure 6. While weaker than Eu^{3+} luminescence, $\mathrm{Sm}^{3+}(^4\mathrm{G}_{5/2})$ emission is still bright and easily observed. By comparison with samples containing only $\mathrm{Sm(Tf_2N)_3}$, it was determined that the spectral properties of Sm^{3+} are unaffected by the presence of $\mathrm{Eu(Tf_2N)_3}$. We note that there is no evidence of significant energy transfer between Sm^{3+} and Eu^{3+}.

The relatively intense $\mathrm{Sm}^{3+}(^4\mathrm{G}_{5/2})$ emission in this sample is consistent with the observed long lifetime. Figure 7 shows the luminescence decay of Sm^{3+} emission at 562 nm, corresponding to the $^4\mathrm{G}_{5/2} \rightarrow {}^6\mathrm{H}_{5/2}$ transition, following 479 nm pulsed excitation. The decay curve is fit very well to a monoexponential function, yielding a lifetime of τ = 430 μs. This is very long lifetime, considering that solution values for Sm^{3+} typically range from τ = 20−50 μs.[46]

The quantum efficiency, η, and radiative lifetime, τ_R, of $\mathrm{Sm}^{3+}(^4\mathrm{G}_{5/2})$ emission were estimated using eqs 1 and 2, respectively, relative to two different secondary standards: R6G in ethanol and $\mathrm{Eu(Tf_2N)_3}$ in bmpyr $\mathrm{Tf_2N}$. For a solution of 1% $\mathrm{Sm(Tf_2N)_3}$ in bmpyr $\mathrm{Tf_2N}$ against an R6G standard, it was determined that η = 0.060 ± 0.012 and τ_R = 5.0 ± 1.0 ms (See Table 1). For a solution of 2% $\mathrm{Sm}^{3+}(^4\mathrm{G}_{5/2})$/2% $\mathrm{Eu(Tf_2N)_3}$ in bmpyr $\mathrm{Tf_2N}$ against the internal $\mathrm{Eu(Tf_2N)_3}$ standard, it was determined that η = 0.095 ± 0.019 and τ_R = 4.53 ± 0.91 ms (See Table 2). The values of τ_R for the two methods are in good agreement, relative to their uncertainties. The difference in η is real, and is due to increased quenching in the 1% $\mathrm{Sm(Tf_2N)_3}$ solution, as manifested in the shorter measured lifetime (compare Table 1 and Table 2). The values of τ_R are consistent with the radiative lifetimes reported for $\mathrm{Sm}^{3+}(^4\mathrm{G}_{5/2})$ in solutions of $\mathrm{Sm(hfa)_3(phen)_2}$ (hfa = hexafluoroacetylacetonato, phen = phenanthoroline), which ranged from τ_R = 2.1−4.3 ms, depending on the solvent.[47]

Using a value of τ_R = 4.7 ms, which is the average of the two values reported above, the quantum efficiency of the $\mathrm{Sm(Tf_2N)_3}$ solutions measured in this study (Table 3), ranged from η = 0.042 to η = 0.11. These quantum efficiencies are quite high for a Sm^{3+} complex in solution. The highest previously reported value that we could find was η = 0.027 for $\mathrm{Sm(hfa)_3(phen)_2}$ in pyridine.[47]

3.6. Luminescence Properties, Quantum Efficiency, and Radiative Lifetime of $\mathrm{Pr}^{3+}(^3\mathrm{P}_0)$ in $\mathrm{Pr(Tf_2N)_3}$ in bmpyr $\mathrm{Tf_2N}$.

The luminescence spectrum of Pr^{3+} in 2% $\mathrm{Pr(Tf_2N)_3}$/2%$\mathrm{Eu(Tf_2N)_3}$ in bmpyr $\mathrm{Tf_2N}$ (444 nm excitation) is shown in Figure 8, and is very similar to that reported for $\mathrm{Pr(Tf_2N)_3}$ in bmpyr $\mathrm{Tf_2N}$ by Babai et al.[15] Emission from both the $\mathrm{Pr}^{3+}(^3\mathrm{P}_0)$ and the $\mathrm{Pr}^{3+}(^1\mathrm{D}_2)$ excited states is observed. By comparison with samples containing only $\mathrm{Pr(Tf_2N)_3}$, it was determined that the spectral properties of Pr^{3+} are unaffected by the presence of $\mathrm{Eu(Tf_2N)_3}$. The $\mathrm{Pr}^{3+}(^3\mathrm{P}_0)$ luminescence decay curve, obtained using 444 nm excitation, is also shown in Figure 8. The decay is monoexponential, and yields a lifetime of 81.3 ns.

For comparison, the emission spectrum of $\mathrm{Eu(Tf_2N)_3}$ obtained from the same sample using 394 nm excitation is shown in Figure 8. The Pr^{3+} and Eu^{3+} spectra in Figure 8 have been corrected for relative excitation intensity. Clearly, considering the different intensity scales used in Figure 8 for the two ions, the Pr^{3+} emission from this sample is much weaker than that of Eu^{3+}.

The quantum efficiency, η, and radiative lifetime, τ_R, of $\mathrm{Pr}^{3+}(^3\mathrm{P}_0)$ emission were estimated using eqs 1 and 2, respectively, relative to two different secondary standards: R6G in ethanol and $\mathrm{Eu(Tf_2N)_3}$ in bmpyr $\mathrm{Tf_2N}$. For a solution of 1% $\mathrm{Pr(Tf_2N)_3}$ in bmpyr $\mathrm{Tf_2N}$ against an R6G standard, it was determined that η = 0.00131 ± 0.00026 and τ_R = 59 ± 12 μs (See Table 1). For a solution of 2% $\mathrm{Pr(Tf_2N)_3}$/2% $\mathrm{Eu(Tf_2N)_3}$ in bmpyr $\mathrm{Tf_2N}$ against the internal $\mathrm{Eu(Tf_2N)_3}$ standard, it was determined that η = 0.00178 ± 0.00036 and τ_R = 45.6 ± 9.1 μs (See Table 2). The values of τ_R for the two methods are in reasonable agreement, relative to their uncertainties. The lower quantum efficiency calculated for 1% $\mathrm{Pr(Tf_2N)_3}$ in bmpyr $\mathrm{Tf_2N}$ is consistent with its shorter measured lifetime (compare Table1 and Table 2), although the difference between η for the two samples is essentially within the range of uncertainty. Consistent with our results, the radiative lifetime of $\mathrm{Pr}^{3+}(^3\mathrm{P}_0)$ emission is known to be quite short in comparison to other Ln^{3+} emitting states. Weber, for example, calculates a radiative lifetime of 3.0 μs for $\mathrm{Pr}^{3+}(^3\mathrm{P}_0)$ in $\mathrm{Y_2O_3}$,[45] and Zaldo et al. calculate a radiative lifetime of 5.8 μs in $\mathrm{KGd(WO_4)_2}$.[48] We have previously reported a $\mathrm{Pr}^{3+}(^3\mathrm{P}_0)$ radiative lifetime of 20 μs in $\mathrm{CsCdBr_3}$.[14]

3.7. Luminescence Properties, Quantum Efficiency, and Radiative Lifetime of $\mathrm{Dy}^{3+}(^4\mathrm{F}_{9/2})$ in $\mathrm{Dy(Tf_2N)_3}$ in bmpyr $\mathrm{Tf_2N}$.

The emission spectrum and luminescence decay curve for Dy^{3+}($^4\mathrm{F}_{9/2}$) in a solution of 2% $\mathrm{Dy(Tf_2N)_3}$/2% $\mathrm{Eu(Tf_2N)_3}$ in bmpyr $\mathrm{Tf_2N}$ are shown in Figure 9. By comparison with samples containing only $\mathrm{Dy(Tf_2N)_3}$, it was determined that the spectral

Table 3. Summary of Luminescence Lifetime Data Obtained for $Ln(Tf_2N)_3$ in bmpyr Tf_2N

excited state	energy gap (cm^{-1})	sample	lifetime (rm temp)	lifetime (77 K)
Er ($^4S_{3/2}$)	3000	0.8% Er	0.15 μs	
Pr($^3P_0$)	3900	0.3% Pr	61.0 ns	
		0.9% Pr	59.6 ns	
		1% Pr	60.0 ns	
		1% Pr	78.7 ns	
		2% Pr/2% Eu	81.3 ns	
Nd($^4F_{3/2}$)	5200	0.3% Nd	26.0 μs	
		1% Nd	25.3 μs	
Tm($^1G_4$)	5800	0.3% Tm	10.3 μs	10.7 μs
		1% Tm	12.0 μs	13.2 μs
Er($^4I_{13/2}$)	6500	0.1% Er	75.0 μs	
		0.3% Er	77 μs	
		0.8% Er	77.0 μs	
		1% Er	70.0 μs	
Tm($^1D_2$)	6600	0.3% Tm	6.4 μs	4.8 μs
		1% Tm	6.3 μs	6.3 μs
		0.6%Eu/0.5%Tm	6.3 μs	
Pr($^1D_2$)	7000	0.3% Pr	1.5 μs	1.7 μs
		0.9% Pr	1.7 μs	
		1% Pr	1.8 μs	
Sm($^4G_{5/2}$)	7200	0.1% Sm	474 μs	
		0.3% Sm	510 μs	472 μs
		1% Sm	259 μs	530 μs
		1% Sm	300 μs	
		2.6% Sm	202 μs	474 μs
		2% Sm/2% Eu	430 μs	
Dy($^4F_{9/2}$)	7900	0.3% Dy	225 μs	267 μs
		1% Dy	244 μs	
		2% Dy	140 μs	
		2% Eu/2% Dy	187 μs	
Eu($^5D_0$)	12200	1% Eu	2.0 ms	
		1% Eu	1.6 ms	2.0 ms
		0.6%Eu/0.5%Tm	1.2 ms	
		2% Eu/2% Pr	1.1 ms	2.0 ms
		2% Eu/2% Dy	1.1 ms	
		2% Eu/2% Sm	1.6 ms	
		4%Eu	1.2 ms	
Tb($^5D_4$)	14300	1% Tb	1.9 ms	

properties of Dy^{3+} are unaffected by the presence of $Eu(Tf_2N)_3$. The $Dy^{3+}(^4F_{9/2})$ decay is very well described by a monoexponential function to yield a lifetime of 187 μs. Again, this is an atypically long lifetime for Dy^{3+} in solution, where lifetimes in the 1−20 μs range are more commonly observed.[46] Even in D_2O, the upper limit on the reported lifetimes is 139 μs.[9] We note that a relatively long lifetime of 63 μs was reported for DyI_3 in the IL $[C_{12}mim]$ Tf_2N.[13]

The quantum efficiency, η, and radiative lifetime, τ_R, of $Dy^{3+}(^4F_{9/2})$ emission were estimated using eqs 1 and 2, respectively, relative to two different secondary standards: R6G in ethanol and $Eu(Tf_2N)_3$ in bmpyr Tf_2N. For a solution of 2% $Dy(Tf_2N)_3$ in bmpyr Tf_2N against an R6G standard, it was determined that $\eta = 0.122 \pm 0.024$ and $\tau_R = 1.14 \pm 0.23$ ms (See Table 1). For a solution of 2% $Dy(Tf_2N)_3$/2% $Eu(Tf_2N)_3$ in bmpyr Tf_2N against the internal $Eu(Tf_2N)_3$ standard, it was determined that $\eta = 0.122 \pm 0.024$ and $\tau_R = 1.53 \pm 0.31$ ms (See Table 2). The values of τ_R for the two methods are in reasonable agreement, relative to their uncertainties. These values are similar to the value of $\tau_R = 1.85$ ms estimated for the Dy^{3+} aquo complex.[49,50] Using a value of $\tau_R = 1.34$ ms, which is the average of the two values reported above, the quantum efficiency of the $Dy(Tf_2N)_3$ solutions measured in this study (Table 3), ranged from $\eta = 0.104$ to $\eta = 0.182$.

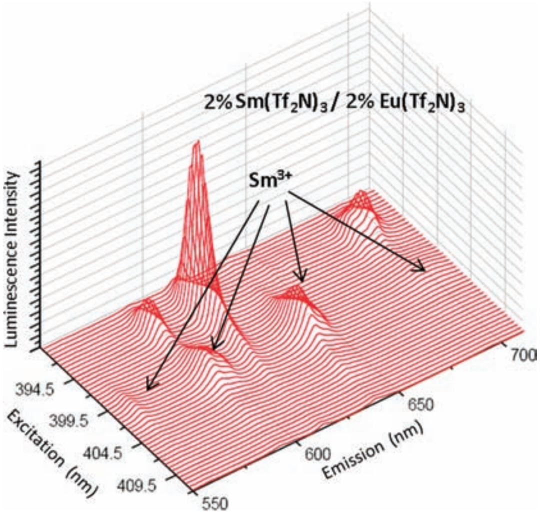

Figure 6. 3D Emission/Excitation mapping of the luminescence properties of 2% $Sm(Tf_2N)_3$ and 2% $Eu(Tf_2N)_3$ in bmpyr Tf_2N. Spectral bandpass of the emission and excitation monochromators was 2 nm.

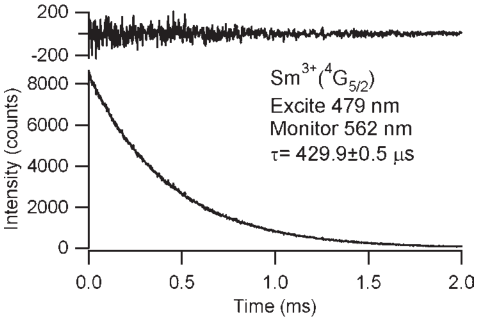

Figure 7. Luminescence decay curve for $Sm^{3+}(^4G_{5/2})$ in 2% $Sm(Tf_2N)_3$/2% $Eu(Tf_2N)_3$ in bmpyr Tf_2N. Residuals for a monoexponential fit are shown above the decay curve plot. The curve was obtained exciting at 479 nm and monitoring emission at 562 nm.

3.8. Luminescence Properties and Lifetime Measurements of $Nd^{3+}(^4F_{3/2})$ in $Nd(Tf_2N)_3$ in bmpyr Tf_2N. A partial NIR emission spectrum of $Nd^{3+}(^4F_{3/2})$ in 1% $Nd(Tf_2N)_3$ in bmpyr Tf_2N is shown in Figure 10. The $^4F_{3/2}\rightarrow{}^4I_{11/2}$ and the $^4F_{3/2}\rightarrow{}^4I_{13/2}$ emission peaks are clearly observed at 1059 and 1335 nm, respectively. The high signal-to-noise ratio in the emission spectrum is indicative of the strong luminescence observed from this sample.

The explanation for the strong emission is found in the relatively long luminescence lifetime of $\tau = 25$ μs, as determined by a monoexponential fit to the decay curve shown in Figure 10. In their review article on lanthanide NIR emission, Comby and

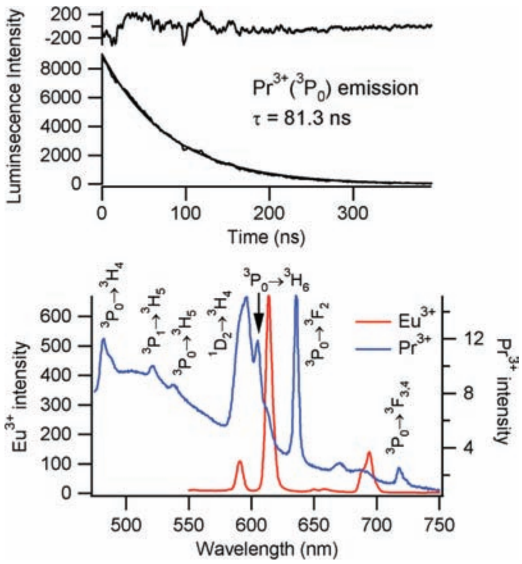

Figure 8. (Lower Plot) Luminescence spectra of Pr^{3+} (blue) and Eu^{3+} (red) in a solution of 2% $Pr(Tf_2N)_3$/2% $Eu(Tf_2N)_3$ in bmpyr Tf_2N. Spectral resolution is 2 nm. For Pr^{3+}, λ_{ex} = 444 nm. For Eu^{3+}, λ_{ex} = 463 nm. (Upper Plot) Luminescence decay curve for Pr^{3+} ($^3P_0$) emission obtained by exciting at 444 nm and monitoring at 636 nm.

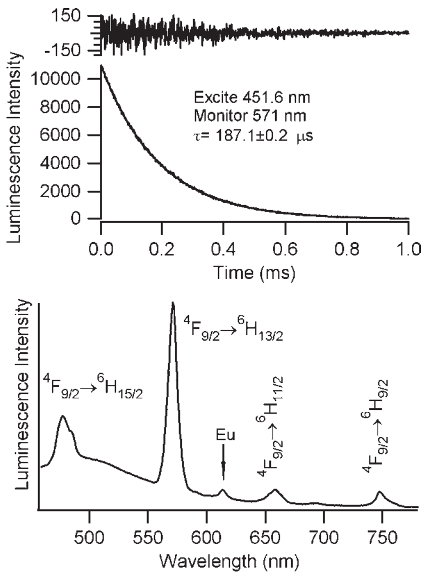

Figure 9. Emission spectrum (bottom) and luminescence decay (top) of $Dy^{3+}(^4F_{9/2})$ in a solution of 2% $Dy(Tf_2N)_3$/2% $Eu(Tf_2N)_3$ in bmpyr Tf_2N. The emission spectrum was obtained using 350 nm excitation. Spectral resolution is 2 nm. The decay curve was obtained exciting at 451.6 nm and monitoring emission at 571 nm.

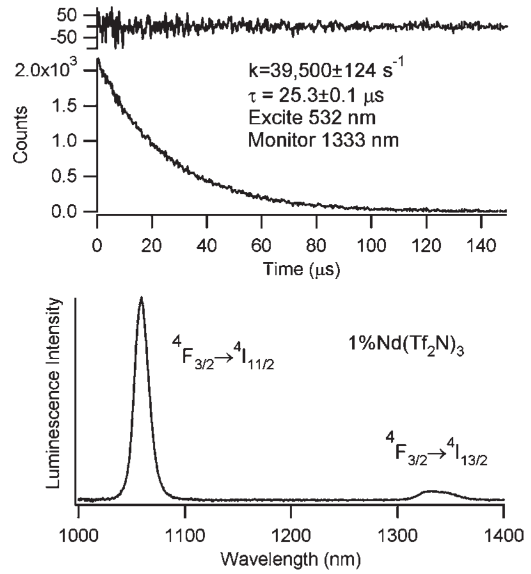

Figure 10. (Lower Plot) Partial NIR emission spectrum of Nd^{3+}-($^4F_{3/2}$) in 1% $Nd(Tf_2N)_3$ in bmpyr Tf_2N obtained using 532 nm excitation. The spectral resolution is 5 nm. (Upper Plot) Decay curve of $Nd^{3+}(^4F_{3/2})$ luminescence at 1333 nm obtained using 532 nm pulsed excitation.

Bünzli compile an extensive table of the lifetimes and quantum efficiencies of Nd^{3+} complexes in solid form, and in aqueous and nonaqueous solutions (for both deuterated and nondeuterated solvents).[50] None of the tabulated systems exhibit lifetimes exceeding 3 μs, and few exhibit quantum efficiencies greater than 1%.

Europium cannot be used as a viable internal standard for quantum efficiencies of the NIR emitters, like $Nd^{3+}(^4F_{3/2})$. It is also difficult to make an accurate estimation of the quantum efficiency of $Nd(Tf_2N)_3$ in bmpyr Tf_2N based on reported values of τ_R, because the radiative lifetime of $Nd^{3+}(^4F_{3/2})$ seems to vary significantly from compound to compound. However, a typical range of radiative lifetimes reported for Nd^{3+} complexes is τ_R = 0.25−1.0 ms,[16,50] which would correspond to a quantum efficiency of η = 2.5−10%, given the measured luminescence lifetime of τ = 25 μs for $Nd(Tf_2N)_3$ in bmpyr Tf_2N.

There are several studies in the literature on the NIR luminescence properties of Nd^{3+} in IL systems. Driesen et al. report the lifetimes of the 1064 nm emission for Nd^{3+} tosylate (TOS), triflate (TfO), bisperfluorobutylsulfonylimide (PBS), and bromide complexes dissolved in 1-alkyl-3-methylimadazolium ILs that contained the same anion as the Nd^{3+} complex.[17] In these systems, the $Nd^{3+}(^4F_{3/2})$ lifetime ranged from τ = 0.38−1.5 μs. It is interesting to note that, for $NdBr_3$ in 1-hexyl-3-methylimidazolium bromide, $[C_6mim]Br$, the measured lifetime of 1.5 μs suggest that either the sample was not adequately dry to prevent quenching by water or the intrinsic multiphonon relaxation in this system is more efficient than for $Nd(Tf_2N)_3$ in bmpyr Tf_2N. If the latter were true, one might suspect that quenching by C_6mim^+ in the second coordination sphere is the dominant multiphonon relaxation pathway, since the phonon cutoff for $[LnBr_x]^{3-x}$ complexes is quite low (<200 cm^{-1}).

In light of our results and those of others discussed above, it is particularly interesting to consider the study of NdI_3 in $[C_{12}mim][Tf_2N]$, for which a lifetime of τ = 15.3 μs and a quantum efficiency of η = 1.5 ± 0.2% was reported.[16] Whether Tf_2N^- or, as the authors suggest,[16] I^-, is the predominate metal-binding ligand, the increased lifetime relative to $NdBr_3$ in $[C_6mim]Br$ could be explained in terms of the larger, nonquenching first coordination sphere "pushing back" the quenching C_nmim^+ cations in the second coordination sphere. In the present case, comparing $Nd(Tf_2N)_3$ in bmpyr Tf_2N to $NdBr_3$ in $[C_6mim]Br$, one would conclude that the quenching by directly coordinated Tf_2N^- ligands, which lack high-frequency C−H vibrations, in the $[Nd(Tf_2N)_x]^{3-x}$ complex is less efficient than

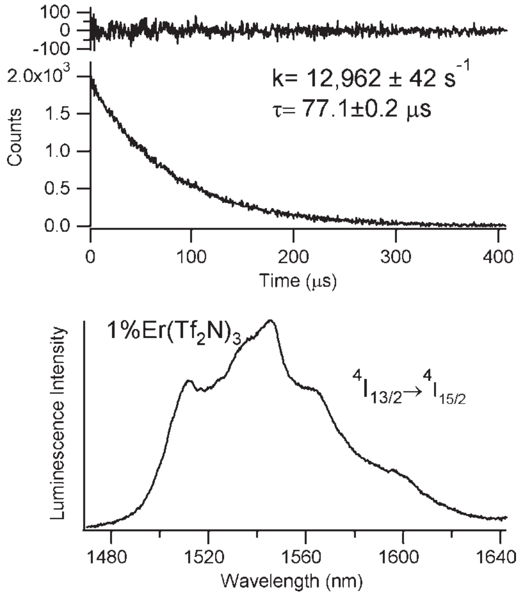

Figure 11. Emission spectrum (Lower Plot) and luminescence decay curve (Upper Plot) corresponding to the NIR $^4I_{13/2}{\rightarrow}^4I_{15/2}$ transition of Er(Tf$_2$N)$_3$ in bmpyr Tf$_2$N. The emission spectrum was obtained using 532 nm continuous wave excitation. Spectral resolution is 2.5 nm. The decay curve was obtained using 522 nm pulsed excitation, monitoring the emission at 1545 nm.

quenching by C$_6$mim$^+$ in the second coordination sphere of [LnBr$_x$]$^{3-x}$. Quenching of the ^{5}D$_0$ emission of Eu^{3+} complexes by second-coordination-sphere water molecules has been observed,[42,51] and appears to follow a R^{-6} dependence, where R is the distance between the water molecule and the Eu^{3+} ion.[51]

3.9. Luminescence Properties and Lifetime Measurements of Er^{3+}(^{4}I$_{13/2}$) in Er(Tf$_2$N)$_3$ in bmpyr Tf$_2$N.

The emission spectrum and luminescence decay curve corresponding to the NIR $^4I_{13/2}{\rightarrow}^4I_{15/2}$ transition of Er(Tf$_2$N)$_3$ in bmpyr Tf$_2$N are shown in Figure 11. The maximum intensity of the transition is observed at 1545 nm. The luminescence decay curve is fit very well to a monoexponential decay function, yielding an extraordinarily long lifetime of $\tau = 77$ μs. For ErI$_3$ in [C$_{12}$mim][Tf$_2$N], Arenz et al. report a lifetime of τ = 10.4 μs.[16] We note, however, that the $^4I_{13/2}{\rightarrow}^4I_{15/2}$ emission spectrum of ErI$_3$ in [C$_{12}$mim][Tf$_2$N] differs significantly from that shown in Figure 11,[16] indicating that the emitting Er^{3+} complex is not the same as in the present system. In our lab, we have measured the $^4I_{13/2}{\rightarrow}^4I_{15/2}$ emission spectrum of ErI$_3$ in bmpyr Tf$_2$N, and note that its features are very similar to that reported for ErI$_3$ in [C$_{12}$mim][Tf$_2$N]. It is, therefore, likely that the emitting Er^{3+} species for ErI$_3$ in both bmpyr Tf$_2$N and [C$_{12}$mim][Tf$_2$N] have I$^-$ in the first coordination sphere.

It is incorrect, however, to assume that I$^-$ will be coordinated to Ln^{3+} for all solutions of LnI$_3$ in bmpyr Tf$_2$N or [C$_{12}$mim][Tf$_2$N]. Babai et al. observe essentially identical emission spectra for solutions of PrI$_3$ and Pr(Tf$_2$N)$_3$ in bmpyr Tf$_2$N, which leads them to assign the emitting species to a [Pr(Tf$_2$N)$_x$]$^{3-x}$ complex in both cases.[15] Our results support their conclusion, in that we measure very similar Pr^{3+}(^{3}P$_0$) and Pr^{3+}(^{1}D$_2$) lifetimes for both PrI$_3$ and Pr(Tf$_2$N)$_3$ salts in bmpyr Tf$_2$N. Moreover, the spectroscopic data we have acquired for SmI$_3$ and DyI$_3$ in bmpyr Tf$_2$N are consistent with that presented herein in Sections 3.5 and 3.7 for the Ln(Tf$_2$N)$_3$ salts.

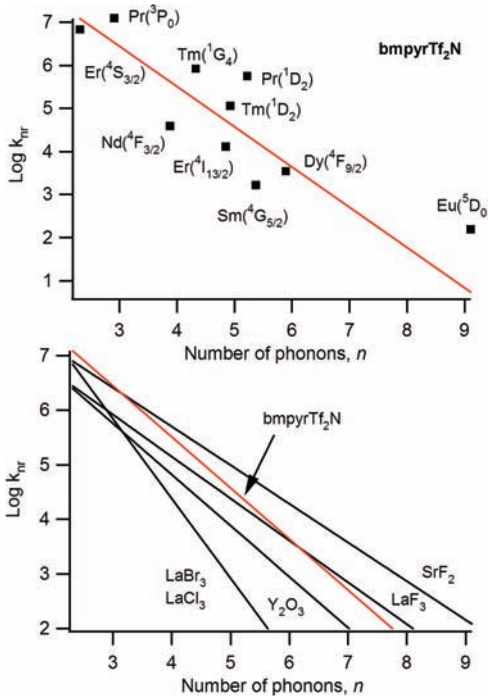

Figure 12. (Upper Plot) log k_{nr} vs n for the observed emitting states of Ln^{3+} in bmpyr Tf$_2$N, where k_{nr} is the multiphonon relaxation rate constant of the emitting state and n is the number of phonons required to bridge the energy gap between the emitting state the lower adjacent state. The red line indicates the best linear fit of the data, excluding Eu^{3+}(^{5}D$_0$). (Lower plot) Comparison of best linear fit to upper plot with multiphonon relaxation behavior of Ln^{3+} in several well-known crystal lattices (as reported in ref 52).

3.10. Multiphonon Relaxation of Ln(Tf$_2$N)$_3$ in bmpyr Tf$_2$N.

Because emission is observed from so many Ln^{3+} excited states in the present system, it is possible to conduct a systematic analysis of multiphonon relaxation. The luminescence lifetime data obtained for Ln(Tf$_2$N)$_3$ in bmpyr Tf$_2$N are summarized in Table 3. Several general comments regarding the data in Table 3 are warranted. First, we note that no clear effect is observed regarding the concentration of Ln(Tf$_2$N)$_3$ on the luminescence lifetime over the range of concentrations used. Second, there is some significant variability in observed lifetime from sample-to-sample for a given Ln^{3+}. This is indicative of the delicate nature of the [Ln(Tf$_2$N)$_x$]$^{3-x}$ complexes in the IL; the weakly coordinating properties of Tf$_2$N$^-$ render the Ln^{3+} ion susceptible to quenching by even small concentrations of contaminating ligands. Finally, we have measured lifetimes for several of the samples at 77 K as a check for the presence of quenching ligands, such as water. Note, for example, that the most variability in the room-temperature lifetime is observed for Sm^{3+}. However, at 77 K, the lifetime of all Sm^{3+} samples is approximately 500 μs, which is close to the longest room-temperature lifetimes. The interpretation of this observation is that, at 77 K, no ligand exchange is possible, and luminescence is observed only from [Ln(Tf$_2$N)$_x$]$^{3-x}$ complexes, because emission from the water-containing complexes, for example, is completely quenched. For the Eu^{3+} samples at 77 K, multiexponential decays were usually observed, because Eu^{3+} emission is not totally quenched by bound water, with the longest-lived component having a lifetime of τ = 2.0 ms. We assign the lifetime of τ = 2.0 ms, which also

Table 4. Comparison of the γ Values, As Defined in eq 6, for bmpyr Tf_2N Compared to Those for SrF_2, LaF_3, Y_2O_3, $LaCl_3$, and $LaBr_3$ Reported by Riseberg and Moos[52]

host	$h\nu_{max}$ (cm^{-1})	γ
SrF_2	360	1.6
LaF_3	350	1.8
bmpyrTf_2N	1340	2.2
Y_2O_3	550	2.2
$LaBr_3$	175	3.4
$LaCl_3$	260	3.4

matches the longest lifetime measured at room temperature, to the unhydrated $[Eu(Tf_2N)_x]^{3-x}$ complex. This is consistent with the room-temperature lifetimes of 1.66 and 1.91 ms reported for the metastable liquid phases of C_3mim[$Eu(Tf_2N)_4$] and bmim-[$Eu(Tf_2N)_4$], respectively.[8]

Multiphonon relaxation within the 4f configuration of Ln^{3+} ions is known to follow the general trend given by the so-called energy-gap law.[52,53]

$$k_{nr} = \beta \cdot e^{-\alpha \cdot \Delta E} \tag{5}$$

where k_{nr} is the multiphonon-relaxation rate constant, ΔE is the energy gap between the emitting state and the lower adjacent state, and α and β are constants for a given crystal lattice, where α is related to the electron−phonon coupling strength.[54] We note that van Dijk and Schuurmans have suggested that the effective energy gap should be reduced by either $2h\nu_{max}$ or $h\nu_{max}$ to obtain a more physically meaningful value of β.[55]

In describing multiphonon relaxation, a more fundamental quantity than the energy gap, ΔE, is the number of phonons, n, required to bridge the energy gap. Equation 5 then becomes

$$k_{nr} = \beta \cdot e^{-\gamma \cdot n} \tag{6}$$

where $n = \Delta E / h\nu_{max}$, $h\nu_{max}$ is the maximum vibrational frequency of the system, and $\gamma = \alpha \cdot h\nu_{max}$. The advantage to eq 6 is that γ is also related to the crystal-field strength and electron−phonon coupling,[52,56] but, unlike α, γ values for different crystal systems, with different values of $h\nu_{max}$, can be directly compared. In the spirit of the modified energy gap law, a more physically meaningful value of β is obtained from eq 6 if n is replaced by $n - 2$.[54,55] Although generally applied to Ln^{3+} ions in crystalline hosts, the energy gap law has also been used to describe quenching in solution, particularly the isotope effect of replacing −OH with −OD moieties.[50,57,58]

A plot of log k_{nr} versus n for all of the observed emitting states of Ln^{3+} in bmpyr Tf_2N is shown in Figure 12. For Eu^{3+}, Sm^{3+}, Tm^{3+}, and Dy^{3+}, the values of k_{nr} were determined by subtracting the radiative rate constants, k_R, reported above, from the observed total rate constants, $k = 1/\tau$. For all other emitting states, the observed lifetimes are short enough to justify the assumption that the radiative rate constants are small relative to the total rate constants, and, therefore, $k_{nr} \approx k$. In all cases, the longest observed room-temperature lifetimes in Table 3 were used to calculate k_{nr}, based on the reasonable assumption that these most closely approximate the lifetimes intrinsic to the $[Ln(Tf_2N)_x]^{3-x}$ complexes. The values of n were calculated assuming a maximum phonon energy of 1340 cm^{-1}, corresponding to the maximum vibrational energy of the Tf_2N^- ligand, which is assigned to the asymmetrical SO_2 stretch. Because we are not analyzing β values, we have chosen here to use the energy gap law, as opposed to the modified energy gap law, to facilitate direct comparison with seminal reports in the literature.

It is seen from the upper plot in Figure 12 that log k_{nr} follows a general linear trend with n, in accordance with the energy-gap law, although the degree of scatter around the best-fit line is much greater than that typically observed for multiphonon relaxation in crystalline hosts. (The best-fit line was obtained excluding the Eu^{3+} datum, since k_{nr} is small and thus the uncertainty in log k_{nr} for this point is large.) The relatively large degree of scatter could be attributable to a number of factors. First, there is no lattice to impose uniformity in either structure or coordination number in the $[Ln(Tf_2N)_x]^{3-x}$ complexes across the Ln^{3+} series. The crystal structures of $[bmpyr]_2[Ln(Tf_2N)_5]$, Ln = Nd, Tb and [bmpyr][$Ln(Tf_2N)_4$], Ln = Tm, Lu, for example, show that the coordination number of the Ln^{3+} changes from 9 to 8 in the transition from the larger Ln^{3+} ions to the smaller.[33] Also, the participation of a second vibrational mode, such as C−H, on the $bmpyr^+$ cation in the outer coordination sphere is a possibility, particularly in light of the higher multiphonon rates observed for $NdBr_3$ in [C_6mim]Br (see Sec. 3.8).

It is interesting to compare the multiphonon relaxation behavior in the present systems to that in well-known crystalline lattices. The lower plot in Figure 12 shows the best-fit line of log k_{nr} versus n for $[Ln(Tf_2N)_x]^{3-x}$ in bmpyr Tf_2N compared to those reported for Ln^{3+} in SrF_2, LaF_3, Y_2O_3, $LaCl_3$, and $LaBr_3$ by Riseberg and Moos.[52] It is seen that the general trend of multiphonon relaxation in the present system is quite consistent with that observed for crystalline hosts, for which adherence to the energy gap law is well established. Table 4 shows a comparison of the γ values for bmpyr Tf_2N compared to those for SrF_2, LaF_3, Y_2O_3, $LaCl_3$, and $LaBr_3$. In general, γ decreases with increasing crystal field strength[52] and electron−phonon coupling.[56] It can be seen that the effective coupling strength of the Ln^{3+} emitting states to the quenching vibrational mode in bmpyr Tf_2N is similar to that in Y_2O_3.

4. CONCLUSIONS

Because of the relative inefficiency of multiphonon relaxation in $[Ln(Tf_2N)_x]^{3-x}$ in bmpyr Tf_2N, luminescence is observed from an unusually large number of Ln^{3+} excited states compared to that normally observed for Ln^{3+} complexes in solution. It was, therefore, possible to determine multiphonon relaxation rate constants, k_{nr}, for a sufficient number of emitting states to perform an energy-gap-law analysis and to compare the results to those reported for well-known crystalline hosts. It was observed that the energy gap law does describe the general trend in multiphonon relaxation, but that the deviations from the trend are much larger than those normally observed for crystal systems. Moreover, the results of the energy gap law analysis are consistent with those reported for crystalline hosts, in the sense that reasonable parameter values are obtained.

It is particularly interesting to note that the vibrational quenching in the present system is significantly less efficient than that reported for $[LnBr_x]^{3-x}$ complexes in [C_6mim]Br. Since it is clear that the maximum vibrational energy for the $[LnBr_x]^{3-x}$ complex is much less than that for $[Ln(Tf_2N)_x]^{3-x}$, we offer the plausible explanation that high-energy vibrational modes on C_6mim^+ play an active role in quenching emission from $[LnBr_x]^{3-x}$. The lack of quenching by $bmpyr^+$ in the present system can then be explained in terms of the expanded coordination sphere of $[Ln(Tf_2N)_x]^{3-x}$

relative to $[LnBr_x]^{3-x}$, which prevents a close approach of the cation to Ln^{3+}.

The appealing intrinsic high luminescence efficiencies observed in the present systems is somewhat offset by the high susceptibility to quenching by even trace water contamination. We have shown here that water introduced into these systems binds essentially quantitatively to Ln^{3+}. This observation is symptomatic of the more general problem that $[Ln(Tf_2N)_x]^{3-x}$ complexes are intrinsically delicate, because of the weakly coordinating nature of Tf_2N^-. On the other hand, ILs with strongly coordinating anions, such a Cl^-, tend to have higher melting points as well as a smaller Ln^{3+} coordination sphere, which facilitates quenching by the IL cation. The challenge, then, is to find suitable ligands which maintain solubility in bmpyr Tf_2N, are more strongly coordinating than water, but maintain the relatively low phonon-energy cutoff of Tf_2N^-.

It is interesting to note that the values for the quantum efficiencies and radiative lifetimes for $Ln(Tf_2N)_3$ in bmpyr Tf_2N obtained using $Eu(Tf_2N)_3$ as an internal secondary standard are consistent with those obtained using rhodamine 6G or quinine sulfate. $Eu(Tf_2N)_3$ is certainly not a perfect standard, in part because it is not possible to use identical excitation wavelengths for the sample and standard. (The fact that reasonable results are obtained is a testament to the ability of modern fluorometers to correct for instrument response.) However, the use of $Eu(Tf_2N)_3$ as an internal standard in the present study proved useful, both in terms of monitoring the dryness of the IL solutions and in terms of providing a consistency check on the radiative lifetimes reported herein.

■ ASSOCIATED CONTENT

Ⓢ Supporting Information. Samples of the results of elemental analysis of the $Ln(Tf_2N)_3$ salts. This material is available free of charge via the Internet at http://pubs.acs.org.

■ AUTHOR INFORMATION

Corresponding Author

*E-mail: smay@usd.edu.

■ ACKNOWLEDGMENT

This material is based upon work supported by the National Science Foundation/EPSCoR Grant 0903804 and by the State of South Dakota. T.K. was supported through the NSF-REU program (CHE-0552687).

■ REFERENCES

(1) Feldmann, C.; Jüstel, T.; Ronda, C. R.; Schmidt, P. J. *Adv. Funct. Mater.* **2003**, *13*, 511–516.

(2) Henning, A. H. *Angew. Chem., Int. Ed.* **2009**, *48*, 3572–3582.

(3) Kaminskii, A. *Phys. Status Solidi A* **2003**, *200*, 215–296.

(4) Eliseeva, S. V.; Bünzli, J. C. G. *Chem. Soc. Rev.* **2010**, *39*, 189–227.

(5) Torimoto, T.; Tsuda, T.; Okazaki, K.; Kuwabata, S. *Adv. Mater.* **2010**, *22*, 1196–1221.

(6) Lunstroot, K.; Nockemann, P.; Van Hecke, K.; Van Meervelt, L.; Görller-Walrand, C.; Binnemans, K.; Driesen, K. *Inorg. Chem.* **2009**, *48*, 3018–3026.

(7) Lunstroot, K.; Baeten, L.; Nockemann, P.; Martens, J.; Verlooy, P.; Ye, X.; Görller-Walrand, C.; Binnemans, K.; Driesen, K. *J. Phys. Chem. C* **2009**, *113*, 13532–13538.

(8) Tang, S.; Babai, A.; Mudring, A. *Angew. Chem., Int. Ed.* **2008**, *47*, 7631–7634.

(9) Mallick, B.; Balke, B.; Felser, C.; Mudring, A. *Angew. Chem., Int. Ed.* **2008**, *47*, 7635–7638.

(10) Samikkanu, S.; Mellem, K.; Berry, M.; May, P. S. *Inorg. Chem.* **2007**, *46*, 7121–7128.

(11) Nagaishi, R.; Arisaka, M.; Kimura, T.; Kitatsuji, Y. *J. Alloys Compd.* **2007**, *431*, 221–225.

(12) Binnemans, K. *Chem. Rev.* **2007**, *107*, 2592–2614.

(13) Mudring, A.-V.; Babai, A.; Arenz, S.; Giernoth, R.; Binnemans, K.; Driesen, K.; Nockemann, P. *J. Alloys Compd.* **2006**, *418*, 204–208.

(14) Gaillard, C.; Billard, I.; Chaumont, A.; Mekki, S.; Ouadi, A.; Denecke, M. A.; Moutiers, G.; Wipff, G. *Inorg. Chem.* **2005**, *44*, 8355–8367.

(15) Babai, A.; Mudring, A. V. *Chem. Mater.* **2005**, *17*, 6230–6238.

(16) Arenz, S.; Babai, A.; Binnemans, K.; Driesen, K.; Giernoth, R.; Mudring, A.-V.; Nockemann, P. *Chem. Phys. Lett.* **2005**, *402*, 75–79.

(17) Driesen, K.; Nockemann, P.; Binnemans, K. *Chem. Phys. Lett.* **2004**, *395*, 306–310.

(18) Billard, I.; Mekki, S.; Gaillard, C.; Hesemann, P.; Moutiers, G.; Mariet, C.; Labet, A.; Bünzli, J. C. G. *Eur. J. Inorg. Chem.* **2004**, *2004*, 1190–1197.

(19) Mudring, A.-V.; Tang, S. *Eur. J. Inorg. Chem.* **2010**, 2569–2581.

(20) Stumpf, S.; Billard, I.; Gaillard, C.; Panak, P. J.; Dardenne, K. *Radiochim. Acta* **2008**, *96*, 1–10.

(21) Billard, I.; Georg, S. *Helv. Chim. Acta* **2009**, *92*, 2227–2237.

(22) Stumpf, S.; Billard, I.; Gaillard, C.; Panak, P. J.; Dardenne, K. *Inorg. Chem.* **2008**, *47*, 4618–4626.

(23) Demas, J. N.; Crosby, G. A. *J. Phys. Chem.* **1971**, *75*, 991–1024.

(24) Fery-Forgues, S.; Lavabre, D. *J. Chem. Educ.* **1999**, *76*, 1260–1264.

(25) Nockemann, P.; Binnemans, K.; Driesen, K. *Chem. Phys. Lett.* **2005**, *415*, 131–136.

(26) Chauvin, A. S.; Gumy, F.; Imbert, D.; Bünzli, J. C. G. *Spectrosc. Lett.* **2004**, *37*, 517–532.

(27) Fischer, M.; Georges, J. *Chem. Phys. Lett.* **1996**, *260*, 115–118.

(28) Eaton, D. F. *Pure Appl. Chem.* **1988**, *60*, 1107–1114.

(29) Parker, C. A.; Barnes, W. J. *The Analyst* **1957**, *82*, 606.

(30) Lutz, H.-P.; Luisi, P. L. *Helv. Chim. Acta* **1983**, *66*, 1929–1935.

(31) Kirby, A. F.; Foster, D.; Richardson, F. S. *Chem. Phys. Lett.* **1983**, *95*, 507–512.

(32) Babai, A.; Mudring, A. V. *Z. Anorg. Allg. Chem.* **2008**, *634*, 938–940.

(33) Babai, A.; Mudring, A.-V. *Dalton Trans* **2006**, 1828–1830.

(34) Babai, A.; Mudring, A.-V. *J. Alloys Compd.* **2006**, *418*, 122–127.

(35) Babai, A.; Mudring, A.-V. *Inorg. Chem.* **2006**, *45*, 4874–4876.

(36) Babai, A.; Pitula, S.; Mudring, A.-V. *Eur. J. Inorg. Chem.* **2010**, 4933–4937.

(37) Hazenkamp, M. F.; Blasse, G. *Chem. Mater.* **1990**, *2*, 105.

(38) de Mello Donegá, C.; Junior, S. A.; de Sá, G. F. *J. Alloys Compd.* **1997**, *250*, 422–426.

(39) Werts, M. H. V.; Jukes, R. T. F.; Verhoeven, J. W. *Phys. Chem. Chem. Phys.* **2002**, *4*, 1542.

(40) Jin, H.; O'Hare, B.; Dong, J.; Arzhantsev, S.; Baker, G. A.; Wishart, J. F.; Benesi, A. J.; Maroncelli, M. *J. Phys. Chem. B* **2007**, *112*, 81–92.

(41) Horrocks, W. D.; Sudnick, D. R. *Acc. Chem. Res.* **1981**, *14*, 384–392.

(42) Supkowski, R. M.; Horrocks, W. D. *Inorg. Chim. Acta* **2002**, *340*, 44–48.

(43) O'Mahony, A. M.; Silvester, D. S.; Aldous, L.; Hardacre, C.; Compton, R. G. *J. Chem. Eng. Data* **2008**, *53*, 2884–2891.

(44) Jayasankar, C. K.; Renuka; Devi, A. *Opt. Mater.* **1996**, *6*, 185–201.

(45) Weber, M. J. *Phys. Rev.* **1968**, *171*, 283.

(46) Hemmilä, I.; Laitala, V. *J. Fluoresc.* **2005**, *15*, 529–542.

(47) Hasegawa, Y.; Tsuruoka, S.; Yoshida, T.; Kawai, H.; Kawai, T. *J. Phys. Chem. A* **2008**, *112*, 803–807.

(48) Zaldo, C.; Rico, M.; Cascales, C.; Pujol, M. C.; Massons, J.; Aguiló, M.; Diaz, F.; Porcher, P. *J. Phys: Condens. Matter* **2000**, *12*, 8531.

(49) *The absorption and fluorescence spectra of rare earth ions in solution*; Carnall, W. T., Ed.; North Holland: Amsterdam, The Netherlands, 1979; Vol. 3.

(50) Comby, S.; Bünzli, J.-C. G. In *Handbook on the Physics and Chemistry of Rare Earths*; Gschneidner, K. A., Jr., Bünzli, J.-C. G., Pecharsky, V. K., Eds.; Elsevier: New York, 2007; Vol. 37, p 217.

(51) May, P. S.; Richardson, F. S. *Chem. Phys. Lett.* **1991**, *179*, 277–281.

(52) Riseberg, L. A.; Moos, H. W. *Phys. Rev.* **1968**, *174*, 429–438.

(53) Weber, M. J. *Phys. Rev. B* **1973**, *8*, 54–64.

(54) Marcantonatos, M. D. *J. Chem. Soc., Faraday Trans. 2* **1986**, *82*, 381–393.

(55) Van Dijk, J. M. F.; Schuurmans, M. F. H. *J. Chem. Phys.* **1983**, *78*, 5317.

(56) Englman, R.; Jortner, J. *Mol. Phys.* **1970**, *18*, 145–164.

(57) Stein, G.; Würzberg, E. *J. Chem. Phys.* **1975**, *62*, 208.

(58) Kimura, T.; Kato, Y. *J. Alloys Compd.* **1998**, *275—277*, 806–810.

NOTE ADDED AFTER ASAP PUBLICATION

This paper was published on the Web on June 15, 2011, with a minor error in Table 4, due to a production error. The corrected version was reposted on June 17, 2011.